

## ARTICLE (Pre-print)

# Open Machine Learning Models for Actual Takeoff Weight Prediction

Mayara C. R. Murça ,<sup>1</sup> Marcos R. O. A. Maximo ,<sup>2</sup> Joao P. A. Dantas ,<sup>3</sup> João B. T. Szenczuk ,<sup>1</sup> Carolina Rutili de Lima ,<sup>2</sup> Lucas O. Carvalho ,<sup>1</sup> and Gabriel A. Melo <sup>2</sup>

<sup>1</sup>Division of Civil Engineering, Aeronautics Institute of Technology, São José dos Campos, Brazil

<sup>2</sup>Autonomous Computational Systems Lab (LAB-SCA), Computer Science Division, Aeronautics Institute of Technology, São José dos Campos, Brazil

<sup>3</sup>Decision Support Systems Subdivision, Institute for Advanced Studies, São José dos Campos, Brazil

\*Corresponding author: mayara@ita.br

## Abstract

Aircraft weight is a key input in flight trajectory prediction and environmental impact assessment tools. However, the lack of openly available data regarding the actual aircraft weight throughout the flight requires the development of mass estimation approaches to be incorporated into these tools. This study uses large-scale open aviation data to develop an open-source machine learning model to predict commercial flights' actual takeoff weight. The data combines detailed flight, trajectory, and meteorological information for 369,013 flights that transited through the European airspace in 2022. Several operational features are created to represent each flight's horizontal and vertical profiles accurately. Model learning explores individual applications of *CatBoost*, *LightGBM*, *XGBoost*, an ensemble of these three models, and artificial neural networks, selected for their robust performance in structured data analysis and potential for high predictive accuracy. The models are evaluated based on their efficiency, accuracy, and applicability to real-world data. The best-performing model is found to predict the aircraft takeoff weights with a mean percentage of error of 1.73%.

**Keywords:** Air Traffic Management; aircraft mass; predictive modeling; machine learning

**Abbreviations:** JOAS: Journal of Open Aviation Science, ATM: Air Traffic Management

## 1. Introduction

Air Traffic Management (ATM) advancements are crucial for achieving a globally sustainable aviation industry. The implementation of novel technologies and operational concepts, such as Trajectory-Based Operations (TBO), have been explored worldwide to reach increasingly stringent environmental performance targets [1]. This requires advanced tools for modeling and predicting flight trajectory performance and its associated environmental impact across multiple scales. To this goal, extensive previous work has explored analytical and empirical approaches for trajectory prediction [2, 3], fuel burn estimation [4, 5, 6] and emissions assessment [7, 8], considering the different phases of the flight operation.

As a fundamental parameter in flight dynamics, aircraft weight is an essential input for these models. However, this information is only available in detailed aircraft data registered by Flight Data Recorder (FDR) systems, being considered proprietary and kept confidential by airlines. This lack of openly available data is typically compensated with assumptions and estimations of aircraft mass, which might introduce a significant source of error and lead to inaccurate trajectory predictions [9].

Previous studies have focused on improving mass estimations with the use of other sources of data, such as aircraft surveillance data. Alliger et al. [10] introduced a least squares method to estimate

the mass from past trajectory points using the physical model of the aircraft and radar data. With the advent of Automatic Dependent Surveillance-Broadcast (ADS-B), flight trajectory data has become increasingly accessible to the general public through flight tracking service providers such as the OpenSky Network [11], allowing for novel data-driven modeling approaches to be explored by researchers. Taking advantage of large-scale historical ADS-B data from the OpenSky Network, Alligier [12] developed a machine learning approach, using neural networks and gradient boosting machines to create predictive models of the mass and speed profile during the climb phase.

Specifically focused on the takeoff phase, Sun et al. [13] used ADS-B data in combination with physical kinetic models to infer aircraft takeoff weight based on two different estimation methods. More recently, the authors [14] developed a Bayesian inference approach to estimate the initial mass at takeoff, using independent aircraft mass estimates at different flight phases computed with analytical models that incorporate trajectory information. However, these approaches still relied on prior knowledge of aircraft dynamics and aircraft performance parameters that are not openly available.

This work aims to develop an open-source machine learning model to predict a flight's actual takeoff weight (ATOW) based on large-scale open aviation data. The machine learning methods applied in this study include *LightGBM*, *CatBoost*, *XGBoost*, an ensemble model combining these algorithms, and artificial neural networks, chosen for their effectiveness in handling structured data and potential for high predictive accuracy. The choice of these methods reflects the popularity of GBDT (Gradient-Boosting Decision Trees) models for tabular data and the versatility of neural networks for complex data patterns. The main motivation for this work was the Eurocontrol Performance Review Commission (PRC) Data Challenge [15], which emphasized the need for open models to support studies assessing the impact of aviation on climate change.

The remainder of this article is organized as follows. Section 2 presents the methodology used to process the data and develop the predictive models. In Section 3, we discuss the results, comparing and analyzing different machine learning models. Finally, Section 4 concludes and shares ideas for future work.

## 2. Method

This section provides a comprehensive overview of the methods used in this study, including data preprocessing, feature engineering, and predictive modeling techniques. We describe the datasets and the steps taken to prepare and enhance them, focusing on how meaningful features were extracted for model learning. The trajectory data processing was developed in R, while the feature engineering and the machine learning models were implemented in Python. Our code is released as open source<sup>1</sup>.

### 2.1 Data Description

This subsection details the open-source datasets used in the study, including flight and trajectory data and supplementary sources that enrich the analysis. These datasets provide essential information on flights, aircraft characteristics, and operational parameters, serving as the basis for building predictive models.

#### 2.1.1 Flight and Trajectory Data

Through the PRC data challenge, Eurocontrol provides the primary data used in this work to predict a flight's actual takeoff weight.

<sup>1</sup><https://github.com/marcosmaximo/prc-challenge-ita>

71  
72  
73  
74  
75  
76  
77  
78  
79  
80  
81  
82

The challenge data made available for model learning is composed of two datasets. The first contains flight data for 369,013 flights that departed or arrived at a European airport in 2022. It provides flight identification, origin, destination airports, aircraft type and wake turbulence category, airline, and operational parameters such as departure and arrival times, flight duration, taxi-out time, flown distance, and the actual takeoff weight (ATOW).

The second dataset provides detailed trajectory data for each flight, including 4D position reports (longitude, latitude, altitude, timestamp), ground speed, track angle, and vertical climb/descent rates. For example, Figure 1 shows the horizontal profile of flight trajectories for one day of operations in the European airspace. Additionally, when available, the dataset provides meteorological data for each 4D position, encompassing the wind components and temperature. It is worth mentioning that flight trajectories are not necessarily complete because of limited ADS-B coverage in some parts of the world and lower altitudes.



Figure 1. Horizontal profile of trajectories flown in the European airspace on April 2, 2022.

The Data Challenge provides a final submission dataset with flight and trajectory data for an additional set of 158,149 flights for ranking the participating teams. We also use this dataset to evaluate the final performance of the models learned based on the predictive performance metrics computed by the Data Challenge organizers.

83  
84  
85  
86

### 2.1.2 Supplementary Data

This study utilized two open-source supplementary datasets to gather airports' geographic coordinates (latitude, longitude) and altitude: the OpenFlights Airports Database<sup>2</sup> and the Global Airport

87  
88  
89

<sup>2</sup>OpenFlights Airports Database: <https://raw.githubusercontent.com/jpatokal/openflights/master/data/airports.dat>

Database<sup>3</sup>. While these sources provided extensive coverage, information about 15 airports in both the challenge and submission sets was still lacking, which we manually added to the dataset to ensure completeness. Additionally, we incorporated an open-source dataset from the Federal Aviation Administration (FAA)<sup>4</sup>, which contains detailed aircraft characteristics. This dataset, updated in September 2023, provides aircraft performance parameters and operational characteristics for our analysis. Furthermore, we created a supplementary database to capture additional aircraft features not present in the FAA dataset. This extra data was compiled manually from public sources, including Wikipedia, technical sheets, factory specifications, and Eurocontrol Data, to enhance the accuracy and completeness of our analysis. For more information on the datasets, refer to the source code of this work.

## 2.2 Data Preprocessing

In this study, trajectory data preprocessing consisted of two main steps: merging datasets and segmenting the flight trajectory into three phases – departure, en route, and arrival. The trajectory data and other flight information were integrated to represent flight trajectories comprehensively. The merging process involved aligning the datasets based on unique flight identifiers and timestamps. This step ensured consistency in each flight record's temporal and spatial attributes, enabling accurate tracking of aircraft positions and speeds over time. In Figure 2, there is an illustration of this process. Also, to analyze the various phases of flight, each trajectory was segmented into three key stages: terminal area departure, en route, and terminal area arrival. We follow the flight phase segmentation currently used for ATM performance analysis, modeling the departure/arrival terminal areas with cylindrical volumes with centers at the origin/destination airports and with a radius of 40 NM/100 NM, respectively.

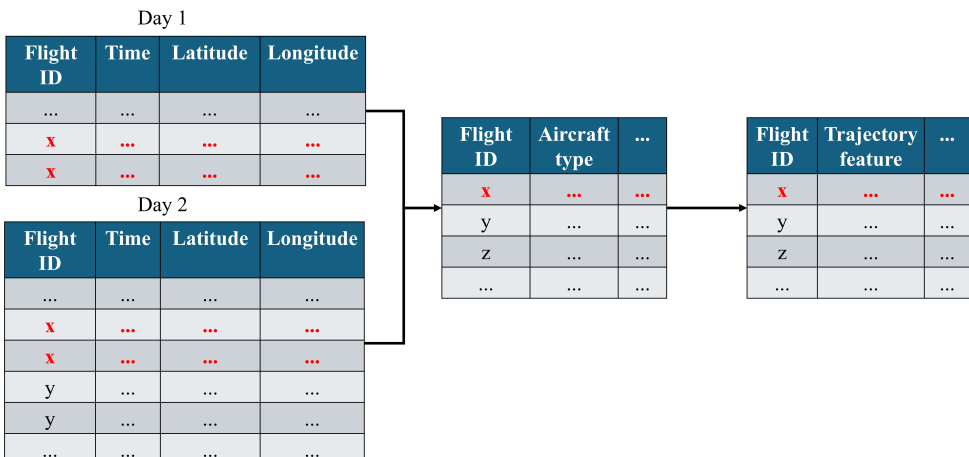


Figure 2. Merging process.

Thus, the departure phase is defined as the segment of the flight trajectory from takeoff until the aircraft exits a 40 NM radius cylinder centered on the departure airport, capturing the aircraft's initial climb and acceleration. The en-route phase represents the flight segment between the departure and arrival cylinders, characterized by the aircraft's cruise altitude and relatively stable speed and heading. The arrival phase corresponds to the flight segment from when the aircraft enters the 100 NM radius cylinder centered on the destination airport until it lands, encompassing the descent

<sup>3</sup>Global Airport Database: <https://www.partow.net/miscellaneous/airportdatabase/>

<sup>4</sup>FAA Aircraft Characteristics Database: [https://www.faa.gov/airports/engineering/aircraft\\_char\\_database/data](https://www.faa.gov/airports/engineering/aircraft_char_database/data)

118  
119  
120  
121  
122  
123

and approach procedures. The segmentation was implemented using a spatial filtering technique that evaluates the aircraft distance from the respective airports, allowing for precise identification of entry and exit points into the cylindrical volumes. This approach ensures that each flight phase is accurately identified, facilitating subsequent analyses of the aircraft behavior in different flight stages. As an example, Figure 3 shows the trajectory of a flight from Lyon–Saint Exupéry Airport (LFLL) to Brussels Airport (EBBR) segmented by flight phase.

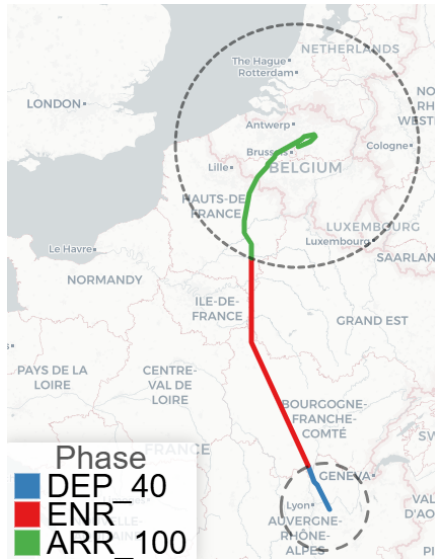


Figure 3. Segmentation of flight phases for an example trajectory.

124  
125  
126  
127  
128

## 2.3 Feature Engineering

129  
130  
131  
132  
133  
134

This subsection details the feature engineering techniques applied to preprocess and enhance the dataset for modeling purposes. The goal was to extract meaningful features that capture temporal patterns, flight characteristics, geographical information, spatial relationships, and interactions between various flight parameters.

135

We engineered several new features to capture horizontal and vertical profile characteristics of flight trajectories, temporal dynamics, flight efficiency, geographical context, and the relationship between different flight parameters. Specifically, we focused on temporal attributes extracted from departure and arrival times, duration-based metrics like taxi ratios and flight speeds, geographical categorizations based on regions and countries, interaction terms combining airspeed and specific energy, and ratio calculations between vertical rate and airspeed.

136  
137  
138

### 2.3.1 Flight Trajectory Features

139  
140  
141  
142

Following identifying flight phases, we created several features to describe the actual trajectory profiles and the meteorological conditions during the operation. For each flight phase (departure, enroute, and arrival), we computed the following aggregate features:

- mean of vertical rate (ft/min), airspeed (m/s), ground speed (kt), temperature (K), humidity (g/kg), and altitude (ft);
- total wind distance (m), i.e., the sum of the products of tailwind/headwind speed and time;
- flown distance (NM);

- specific energy at the last data point ( $V^2 + gh$ , where  $V$  is the airspeed (m/s),  $g$  is the gravity acceleration ( $m/s^2$ ) and  $h$  is the height (m)).

Specifically for the departure phase, we enriched the dataset with the time series of airspeed, temperature, height relative to the origin airport, specific energy, and vertical rate for the first ten observations after takeoff. Additionally, we included information regarding the efficiency of the vertical profile from takeoff until the top-of-climb. For this, we computed the total time (min) and distance flown (NM) in level flight, as level-off segments tend to generate higher fuel burn. Particularly in the departure phase, these level segments might be more probably associated with structural inefficiencies rather than operational inefficiencies, potentially being accounted for during fuel planning. To compute the vertical efficiency during the climb, we follow Eurocontrol's methodological approach [16]. For the trajectory portion within 200 NM from the origin airport and 3,000 ft above ground level, we identify the highest altitude reached as the Top-of-Climb (TOC). An exclusion box is defined around the portion of the vertical profile for which the altitude is greater than or equal to 90% of the TOC. Climb segments with a rate of climb smaller than or equal to 300 ft/min are then identified as level-off segments, provided they occur outside the exclusion box if lasting more than 5 minutes. The distance and time flown in level segments are calculated and summed to produce the features. The approach is illustrated in Figure 4.

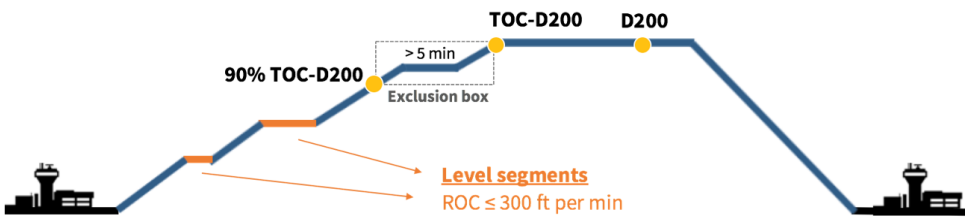


Figure 4. Illustration of the identification of level segments during climb for vertical efficiency quantification.

Finally, we created additional features to describe operational features that are expected to be correlated with the aircraft's takeoff weight based on prior literature. These include the specific energy at the distance of 10 NM flown [17] and the liftoff airspeed and groundspeed [14].

### 2.3.2 Temporal Features

From the departure time, we extracted attributes such as the hour of departure, day of the week, month, week of the year, and the season – categorized into Winter, Spring, Summer, or Fall based on the month. This allowed us to capture daily, weekly, and seasonal patterns that could influence flight operations. For example, flights departing during peak hours or specific seasons might experience different conditions affecting performance. Additionally, we created boolean flags based on the departure time to indicate whether the flight departed on weekends or during rush hours (defined as 7–9 AM or 4–6 PM based on our exploratory data analysis). These features help assess the impact of higher traffic volumes on flight performance.

### 2.3.3 Duration-Based Features

We engineered several duration-based features to capture aspects of flight efficiency and performance. We calculated the ratio of taxi-out time to flight duration, known as the taxi ratio, which assesses the proportion of time spent taxiing relative to the total flight duration. A high taxi ratio might indicate congestion at the airport or inefficiencies in ground operations. We normalized the taxi ratio by dividing it by the median, facilitating comparison across flights.

We also calculated the average speed of the flight by dividing the flown distance by the flight duration. This feature helps analyze operational efficiency over different distances and durations. To maintain data consistency, missing values in flight speed were filled with the median.

To categorize flights based on duration, we introduced a flight duration category by binning the flight durations into Very Short (0–60 minutes), Short (60–180 minutes), Medium (180–300 minutes), and Long (over 300 minutes). This categorization aids in segmenting flights for analysis and modeling purposes.

Additionally, we computed the speed per distance by dividing the flight speed by the flown distance. This feature provides a normalized speed metric relative to the flight distance, assisting in analyzing speed efficiency over varying distances.

#### 2.3.4 Geographical Features

Using the Haversine formula to incorporate geographical context and spatial relationships, we calculated the distance between the departure and arrival airports. It computes the great circle distance between two points on the Earth's surface based on their latitudes and longitudes. This resulted in a new feature representing the actual distance of the flight path. We also calculated the altitude difference between the arrival and departure airports to capture the vertical distance traversed during the flight. The bearing between the two airports was computed to determine the initial compass direction from the departure airport to the arrival airport. Additionally, we calculated the elevation gradient by dividing the altitude difference by the actual distance, representing the altitude change rate per kilometer. These features can influence fuel consumption and flight performance.

Furthermore, we performed clustering based on the departure and arrival airports' geographical coordinates (latitude and longitude). By combining these coordinates and applying the K-Means clustering algorithm, we aimed to identify spatial groupings of airports. We also grouped airports by region based on their country codes, assigning the departure and arrival airports to regions such as Europe, North America, South America, the Middle East, Asia, Africa, and others. This regional classification facilitates the analysis of patterns and differences in flight operations across regions. We developed features to indicate whether a flight was domestic or international. Another feature captured whether the flight occurred within the same geographical area, helping to identify flights that may share common air traffic control procedures or weather patterns.

To capture the flight direction, we created a feature that categorizes flights based on the regions of the departure and arrival airports. This classification enables the analysis of common flight routes and directional trends, offering insights into regional air traffic patterns. We also introduced a feature to identify intercontinental flights, which helps differentiate flights with varying characteristics due to longer distances, diverse regulations, and different airspace complexities.

#### 2.3.5 Interaction Features

We created interaction features to capture the combined effects of certain flight parameters. Specifically, we multiplied the average airspeed by the specific energy during different flight phases, resulting in new variables for the arrival, departure, and en route phases. These features help us understand how an aircraft's speed influences its energy efficiency during different stages of flight.

#### 2.3.6 Binning Continuous Variables

We discretized certain continuous variables into bins to manage the effects of outliers and capture potential nonlinear relationships. We created temperature bins by categorizing the average temperature during the arrival phase into five equal-frequency categories. This allows the model to capture the impact of temperature variations on flight operations without being overly sensitive to extreme

values. Similarly, we created humidity bins by categorizing the average humidity during the departure phase into five categories. Binning these variables facilitates the detection of patterns and thresholds in how temperature and humidity affect flight performance.

### 2.3.7 Ratio Features

We engineered ratio features to analyze the relationship between vertical rate and airspeed during flight phases. The vertical rate indicates the rate of climb or descent, while the airspeed reflects the horizontal speed. The ratios provide insights into the aircraft's climb or descent efficiency relative to its speed during the arrival and departure phases.

## 2.4 Predictive Models

Given the popularity of machine learning models, there are many techniques available. To select which ones we would consider, we used our prior experience as machine learning practitioners and researchers together with knowledge from the literature [18, 19].

Despite Deep Learning dominating perception tasks and big data regimes, machine learning practitioners have noticed that Gradient-Boosted Decision Trees (GBDT) often outperform neural networks on tabular data [19]. In fact, the winning solutions usually employ GBDTs in Data Science competitions. In this regard, the methods XGBoost [20], CatBoost [21], and LightGBM [22] are especially popular [19]. In [23], Abdullahi *et al.* compare these algorithms according to the main features such as speed, scalability, and memory. These comparisons are in Table 1. Therefore, inspired by our experience and the benchmark provided by [19], we decided to evaluate these three GBDT methods and neural networks to learn our predictive models.

**Table 1.** Comparison of CatBoost, LightGBM, and XGBoost

Feature	CatBoost	LightGBM	XGBoost
Categorical Feature Handling	Best at handling categorical variables automatically.	Requires pre-processing for categorical variables.	Requires pre-processing for categorical variables.
Overfitting Robustness	Less prone to overfitting due to symmetrical trees.	Prone to overfitting if not careful with parameters.	Regularization helps prevent overfitting effectively.
Speed	Slower, especially on large datasets.	Fastest due to histogram-based algorithms.	Fast but generally not as fast as LightGBM.
Scalability	Good but less optimal for extensive datasets.	Excellent scalability to large datasets and high-dimensional data.	Good scalability, especially with system optimizations for parallel processing.
Memory Usage	Moderate	Low due to efficient data handling.	High, especially with large data sets.
Ease of Use	Easier with default settings handling categorical data well.	Requires careful data preparation and parameter tuning.	Requires significant parameter tuning and understanding of boosting.
Data Size Handling	Handles small datasets well.	Not as effective with small datasets.	Effective with both large and small datasets but requires tuning.

We standardized parts of our training pipeline to ensure a fair comparison between the machine

learning methods. We separated the dataset into training and test sets with an 80-20 split using the same random seed for every technique. Since the trajectory data was incomplete for all flights, some of the trajectory features presented missing values. Therefore, we tried different methods of data imputation. Experimentally, we found that using the median of the valid elements of the respective column worked the best, outperforming more advanced techniques, such as linear regression and k-NN. This behavior was consistent across the different learning algorithms.

Furthermore, we executed hyperparameter optimization through the Optuna library [24] for each method. Additionally, we implemented early stopping to prevent overfitting and enhance model generalization. During training, the process halts if there is no improvement in the validation performance metric after 50 iterations, helping to avoid excessive fitting to the training data and ensuring robust performance on new data. Specific details of each learning algorithm are presented in the following subsections.

#### 2.4.1 Artificial Neural Networks

This study employed two distinct artificial neural network architectures: a feedforward neural network implemented via FastAI's Tabular learner and the Self-Attention and Intersample Attention Transformer (SAINT) model. These approaches represent different levels of complexity in tabular data processing, each with its own merits in terms of performance and computational requirements.

The FastAI Tabular learner implements a feedforward neural network optimized explicitly for tabular data. The architecture comprises an embedding layer for categorical variables, a preprocessing module for continuous variables, multiple fully connected layers, and an output layer. The embedding layer transforms categorical variables into dense vector representations, with the embedding dimensionality  $d$  for each variable determined by the formula:  $d = \min(600, \text{round}(1.6 * n\_categories^{0.56}))$ , where  $n\_categories$  is the number of unique categories in the variable. This adaptive dimensionality ensures appropriate representational capacity based on the cardinality of each categorical variable.

Continuous variables undergo standardization and, optionally, batch normalization to mitigate internal covariate shifts. The network's core consists of a fully connected layer sequence with Rectified Linear Unit (ReLU) activation functions. These layers can be customized regarding width and depth and may incorporate batch normalization and dropout regularization to enhance generalization. The output layer's architecture is task-dependent, utilizing a single unit with sigmoid activation for binary classification or multiple units with softmax activation for multi-class problems.

The Tabular learner incorporates several advanced optimization techniques. It employs a learning rate finder to determine optimal learning rate ranges, implements discriminative learning rates to allow differential learning speeds across network layers, and utilizes cyclical learning rate schedules to improve convergence characteristics and generalization performance.

In contrast, the SAINT model represents a more advanced approach, leveraging recent developments in transformer architectures. SAINT's primary innovation lies in its dual attention mechanism, which combines self-attention within samples and intersample attention across different samples in a mini-batch. This mechanism enables the model to capture complex intra and inter-sample interactions, potentially leading to more nuanced feature representations.

SAINT initially projects categorical and continuous variables into a unified embedding space, facilitating interactions between different feature types. The embedded representations are then processed through a stack of transformer encoder blocks. Each block comprises self-attention and intersample attention layers, followed by feed-forward networks. This architecture enables iterative refinement of representations, capturing increasingly complex patterns in the data.

A notable feature of SAINT is its ability to utilize contrastive pre-training. This unsupervised learning technique enhances the model's ability to learn robust representations by contrasting similar and dissimilar samples. The pre-training phase can be particularly advantageous in semi-supervised scenarios or when dealing with limited labeled data.

Empirically, SAINT has demonstrated superior performance on various tabular datasets, often surpassing traditional gradient-boosting methods and other neural network approaches. Its capacity to capture intricate relationships in the data renders it particularly suitable for complex tabular problems where simpler models may be inadequate.

The choice between the FastAI Tabular learner and SAINT depends on various factors, including dataset complexity, available computational resources, model interpretability requirements, and specific performance criteria. The Tabular learner offers a more straightforward and computationally efficient approach, suitable for scenarios where interpretability is essential or computational resources are constrained. Conversely, SAINT provides a more robust and flexible approach, capable of modeling highly complex interactions in the data, albeit at the cost of increased computational complexity and potentially reduced interpretability.

Both models offer distinct advantages in the domain of tabular data analysis. An appropriate model should be selected based on carefully considering the task's specific requirements and constraints, potentially necessitating empirical evaluation of both approaches to determine the optimal solution.

#### 2.4.2 CatBoost

According to Hancock and Khoshgoftaar [21], CatBoost is an open-source, GBDT implementation optimized for effectively handling categorical data in supervised machine learning scenarios. Moreover, it introduces two main innovations: 1) Ordered Boosting, which enhances the handling of the order in which data is processed to avoid overfitting; 2) Ordered Target Statistics, a technique to process categorical variables by calculating statistics on the target variable. These features allow CatBoost to manage categorical data more efficiently than popular GBDT implementations like XG-Boost or LightGBM, which often require extensive preprocessing to convert categorical data into numerical formats.

To optimize CatBoost's hyperparameters with Optuna [24], we used the Tree-structured Parzen Estimator (TSE) algorithm and the ranges presented in Table 2. Notice that the value for `reg_lambda` is searched in a logarithmic scale. Despite the `learning_rate` being an important hyperparameter, it is relatively easy to tune manually while significantly impacting the model's performance. We noted that a smaller `learning_rate` generally resulted in a better model but took much longer to train. Hence, we decided to use a fixed `learning_rate` of 0.05 during the hyperparameter search for a maximum of 10,000 iterations. Then, we reduce it to 0.01 when training the final model for a maximum of 50,000 iterations. Furthermore, we employed early stopping with 50 of patience.

Finally, we extensively used the feature selection mechanism of CatBoost to determine which features should be eliminated from the model. Combining hyperparameter optimization and feature selection (both manually and through CatBoost's `select_features()`), we could improve model performance considerably.

#### 2.4.3 Light Gradient-Boosting Machine

LightGBM, or Light Gradient Boosting Machine, in Ke et al. [22], is an efficient GBDT framework designed for distributed and efficient learning, particularly for large-scale and high-dimensional data.

According to Ke et al. [22], LightGBM offers several advantages and innovative features compared

**Table 2.** CatBoost hyperparameters and corresponding ranges used in Optuna.

Hyperparameter	Range	Type	Log Scale
reg_lambda	$[10^{-5}, 100]$	float	Yes
random_strength	$[10, 50]$	float	No
depth	$[1, 15]$	int	No
min_data_in_leaf	$[1, 30]$	int	No
leaf_estimation_iterations	$[1, 15]$	int	No

to traditional gradient boosting methods: 1) Gradient-based One-Side Sampling improves the data sampling process. It ensures that the most informative instances with larger errors (and thus more significant gradients) are used for learning, enhancing the model's efficiency without compromising accuracy; 2) Exclusive Feature Bundling: reduces the dimensionality by bundling mutually exclusive features in high-dimensional data, many features are sparse, which means they contain primarily zeros; 3) Efficient Handling of Categorical Features: handles categorical features by value mapping, which is more efficient than the one-hot encoding used by many other algorithms; and 4) Leaf-wise Tree Growth: grows trees leaf-wise and chooses the leaf that minimizes the loss for growth, allowing for better fitting models, often resulting in increased accuracy with fewer leaves.

Like CatBoost, LightGBM uses the Optuna [24] to tune the best hyperparameter, Table 3. The training of the LightGBM model with Optuna involved setting up an early stopping mechanism and logging the evaluation results during each iteration.

**Table 3.** LightGBM hyperparameters and corresponding ranges used in Optuna.

Hyperparameter	Range	Type	Log Scale
learning_rate	$[1e-3, 0.1]$	float	Yes
max_depth	$[3, 15]$	int	No
min_child_weight	$[1, 10]$	int	No
colsample_bytree	$[0.4, 1.0]$	float	No
reg_alpha	$[1e-4, 1.0]$	float	Yes
reg_lambda	$[1e-4, 1.0]$	float	Yes
n_estimators	1,000,000	int	No

#### 2.4.4 Extreme Gradient Boosting

Extreme Gradient Boosting (XGBoost) is a highly efficient, scalable machine learning system for tree-based boosting, developed initially by Chen and Guestrin [20]. This algorithm builds upon traditional gradient boosting by introducing optimizations that make it particularly effective for large-scale and high-dimensional data. One of its core strengths is its ability to handle sparse data efficiently, allowing it to manage missing or zero-filled values without imputation.

XGBoost incorporates a weighted quantile sketch algorithm to accommodate diverse data distributions. This algorithm approximates quantiles where data points carry different weights or significance. This feature is especially beneficial for datasets with varying data densities and for models that need to prioritize certain data instances, such as in imbalanced classification tasks.

Additionally, XGBoost leverages parallelized tree construction and distributed computing capabilities, enabling it to handle massive datasets while maintaining low training times. It integrates regularization techniques, such as L1 and L2 regularization, which help reduce overfitting and improve the model's generalizability. These combined features make XGBoost one of the top choices for

machine-learning competitions and real-world applications, often outperforming other algorithms in accuracy and computational efficiency.

Key hyperparameters for XGBoost include `learning_rate`, `max_depth`, `min_child_weight`, `gamma`, `colsample_bytree`, `reg_alpha`, and `reg_lambda`. Each of these influences the model's complexity, regularization, and generalization ability. Optimizing these parameters is important to achieve low error rates, and they were fine-tuned using a trial-based approach to minimize the RMSE.

The `learning_rate` controls the step size at each iteration, balancing convergence speed and the risk of missing the global minimum. The `max_depth` hyperparameter determines the maximum depth of each tree, impacting both model complexity and potential overfitting. The `min_child_weight` value is the minimum sum of instance weights needed to split a node, controlling overfitting by limiting intense trees. The `gamma` parameter introduces a minimum loss reduction for further partitioning, creating a threshold for additional split operations.

For feature sampling, `colsample_bytree` specifies the fraction of features to be randomly sampled at each tree, helping reduce the correlation between trees and increase model robustness. The `reg_alpha` and `reg_lambda` variables add L1 and L2 regularization terms, respectively, controlling the model's complexity and penalizing large coefficients to prevent overfitting. Table 4 summarizes the values used during the hyperparameter optimization process.

**Table 4.** XGBoost hyperparameters, corresponding ranges, and descriptions used in Optuna optimization.

Hyperparameter	Range	Description
<code>learning_rate</code>	[0.001, 0.1]	Step size per iteration
<code>max_depth</code>	[3, 15]	Max tree depth
<code>min_child_weight</code>	[1, 10]	Minimum instance weight sum for a node split
<code>gamma</code>	[0.001, 1.0]	Minimum loss reduction for splits
<code>colsample_bytree</code>	[0.4, 1.0]	Feature fraction for sampling per tree
<code>reg_alpha</code>	[0.0001, 1.0]	L1 regularization parameter
<code>reg_lambda</code>	[0.0001, 1.0]	L2 regularization parameter

#### 2.4.5 Ensemble

According to [25], ensemble methods are learning algorithms that combine multiple models to make predictions on new data by aggregating their outputs. While ensembles are widely used in classification and regression tasks, our focus is on regression, which aims to predict continuous values.

The theoretical justification for ensemble methods in regression can be understood through the bias-variance decomposition of the expected Mean Squared Error (MSE). For any predictor  $h(x)$ , the expected MSE can be decomposed as:

$$\mathbb{E}[(y - h(x))^2] = \text{Bias}[h(x)]^2 + \text{Var}[h(x)] + \sigma^2,$$

where  $\sigma^2$  is the irreducible error. When combining multiple models in an ensemble, if the individual models have similar biases but are diverse in their predictions (their errors are not perfectly correlated), the variance component of the error can be reduced while maintaining the bias. For  $m$  models with equal weights  $\frac{1}{m}$ , assuming equal variances  $\sigma_h^2$  and average correlation  $\rho$  between model predictions, the variance of the ensemble becomes:

$$\text{Var}[f_{\text{ensemble}}] = \frac{\sigma_h^2}{m}(1 + (m - 1)\rho).$$

This theoretical foundation motivates the use of weighted ensembles, where each model  $h$  in the hypothesis space  $\mathcal{H}$  outputs a continuous prediction  $h(x)$  for an input  $x$ . The ensemble combines these predictions through a weighted sum to produce the final prediction  $f_{\text{ensemble}}(x)$ :

$$f_{\text{ensemble}}(x) = \sum_{h \in \mathcal{H}} w_h h(x),$$

where  $w_h$  represents the weight assigned to model  $h$ , and  $\sum_{h \in \mathcal{H}} w_h = 1$ .

The optimal weights  $w_h$  can be viewed as the solution to a constrained optimization problem that minimizes the empirical risk on the validation set. In our approach, we use Quadratic Programming (QP) to find these weights by minimizing the MSE while ensuring the sum of the weights equals one:

$$\begin{aligned} \min_w \quad & \frac{1}{n} \sum_{i=1}^n \left( y_i - \sum_{h \in \mathcal{H}} w_h h(x_i) \right)^2 \\ \text{subject to} \quad & \sum_{h \in \mathcal{H}} w_h = 1, \\ & w_h \geq 0, \quad \forall h \in \mathcal{H}. \end{aligned}$$

The QP optimization learns the relative importance of each model's predictions, potentially capturing their complementary strengths while accounting for correlations between their predictions.

## 2.5 Predictive Performance Evaluation

To evaluate the performance of our predictive models, we used the Root Mean Squared Error (RMSE) as the primary metric, given its suitability for regression problems and sensitivity to large errors, which is essential in applications requiring high predictive performance. RMSE measures the average squared differences between predicted and actual values:

$$\text{RMSE} = \sqrt{\frac{1}{n} \sum_{i=1}^n (y_i - \hat{y}_i)^2}, \quad (1)$$

where  $y_i$  and  $\hat{y}_i$  are the  $i$ -th actual and predicted values, respectively. Additionally, we computed the Mean Absolute Percentage Error (MAPE) to obtain a more intuitive estimate of the prediction error as a percentage of the actual output. Mathematically, MAPE is defined as

$$\text{MAPE} = \frac{1}{n} \sum_{i=1}^n \left| \frac{y_i - \hat{y}_i}{y_i} \right| \times 100 \quad (2)$$

## 3. Discussions

This section presents a detailed discussion of the study's key findings. We begin with an exploratory data analysis to identify patterns and trends in the data. Next, we evaluate the predictive performance of the models, followed by an analysis of the importance of features to understand the factors influencing model predictions. Lastly, an ablation study is conducted to assess the contribution of different model components to overall performance.

### 3.1 Exploratory Data Analysis

We performed an exploratory analysis of the flight dataset to understand its characteristics better. Figure 5 shows the total number of flight observations for each month of 2022, and Figure 6 depicts the hourly distribution of actual departure times. The monthly distribution reveals that August 2022 accounted for the maximum number of flights, likely due to the increased demand volume typically seen for the European summer vacation period. By contrast, the lowest number of operations was observed for February 2022. The hourly distribution indicates that traffic departing from European airports rises in the early morning, reaching the peak at 9:00 UTC, when it decreases until around 13:00 UTC. Traffic builds up again in the afternoon, peaking at 16:00 UTC, before gradually declining until the end of the day.

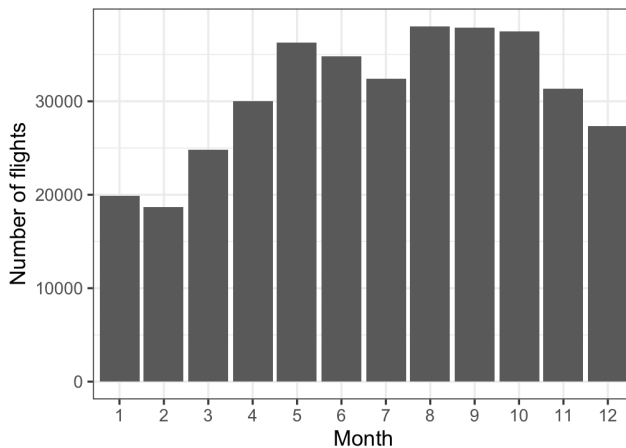


**Figure 5.** Total number of flight observations per month.

Regarding spatial coverage, the flight data contains observations for 4,228 origin-destination (OD) pairs, as shown in Figure 7. Most of the flights are within the European airspace, but the data also contains international flights between Europe and North, Central and South America, Africa, the Middle East, and Asia. The maximum number of 2,157 European flights was observed between London Heathrow Airport (EGLL) and Dublin International Airport (EIDW). Among the international routes, John F. Kennedy International Airport (KJFK) and London Heathrow Airport (EGLL) accounted for the maximum number of 763 flight observations.

The flights in the dataset were operated by 29 airlines using 30 different aircraft types, all pertaining to medium or heavy wake turbulence categories. Figures 8 and 9 show each airline and equipment's percentage share of flight operations. More than 80% of flights were operated by six different airlines, with two airlines concentrating more than 40% of the operations. In terms of equipment, the distribution is slightly less uneven, with more than 80% of the flights executed with ten different types of aircraft. The A320 was the most used equipment, representing 21.6% of the observations.

Figure 10 presents the distribution of ATOW for each aircraft type. As expected, the lowest ATOW was observed for the only medium turboprop aircraft (AT76). Among the medium jets, B752 showed the highest ATOW, while CRJ9 showed the lowest. Heavy jets were inherently associated with the highest levels of ATOW. However, we observed a very high variability for some equipment, such as the B77W. Figure 11 reveals that route length does not explain a significant part of this variability.

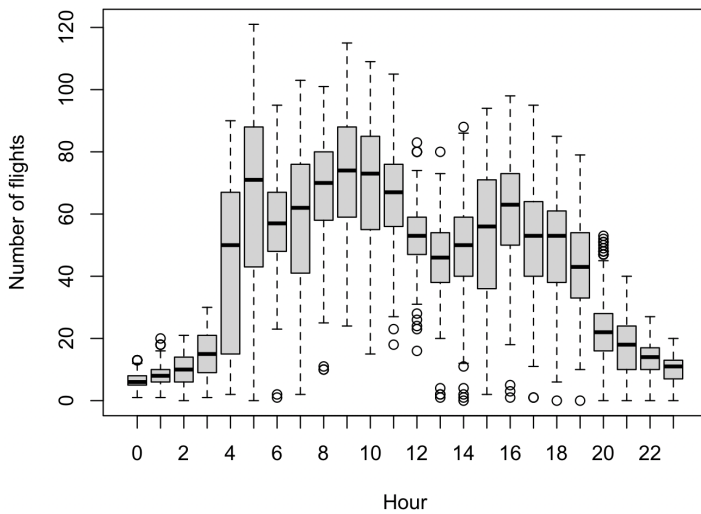


Figure 6. Hourly traffic distribution.

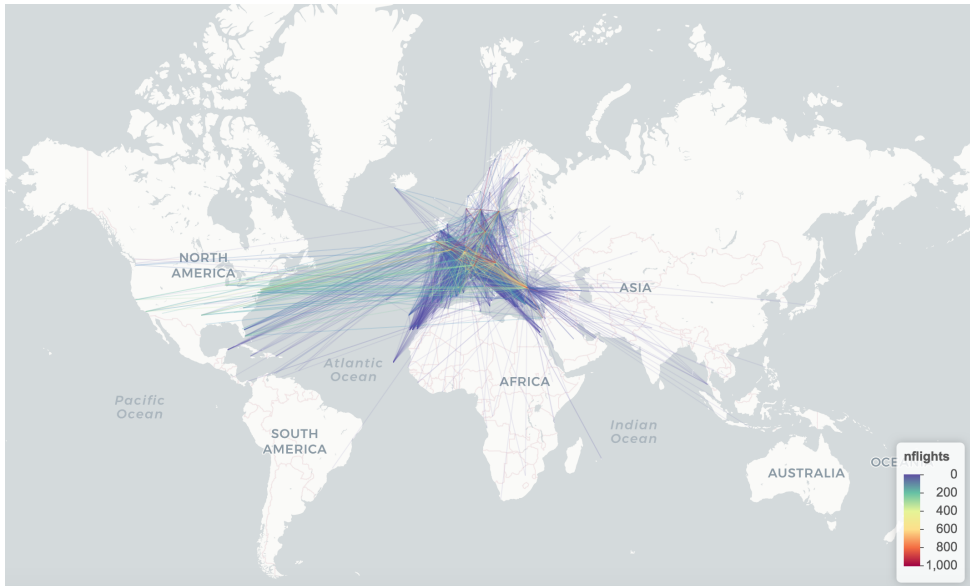


Figure 7. Origin-destination pairs and corresponding number of flight observations.

### 3.2 Predictive Performance Analysis

This subsection presents the predictive performance analysis of five algorithms: XGBoost, CatBoost, LightGBM, ANN, and an ensemble combining all models. The study focuses on key metrics, including the best hyperparameters identified through optimization and the estimated RMSE and MAPE for the test dataset. We also present the actual RMSE for the final submission dataset provided by the Data Challenge to rank the participating teams.

438  
439  
440  
441  
442  
443

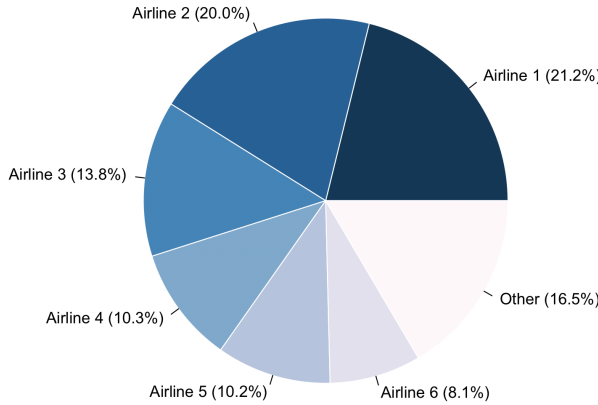


Figure 8. Share of flight operations by airline.

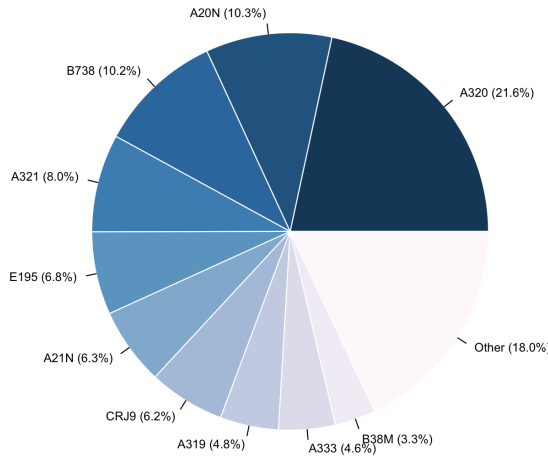


Figure 9. Share of flight operations by aircraft type.

The ensemble model combines predictions from the individual models, leveraging their complementary strengths to achieve improved predictive accuracy. As shown in Table 5, the ensemble model achieved the best test RMSE at 2210.37 and the lowest MAPE at 1.73%, both marked as the lowest errors among the models tested. The actual RMSE values for each algorithm align closely with their estimated test RMSE, indicating that the models generalize well to unseen data.

Among individual models, CatBoost achieved the lowest test RMSE at 2215.53 and MAPE of 1.75%, closely followed by LightGBM and XGBoost, which also demonstrated competitive RMSE and MAPE performance. Although the ANN model performed reasonably, it showed a slightly higher RMSE and MAPE compared to the gradient-boosted models, highlighting the effectiveness of GBDT models on tabular data for this task.

444

445

446

447

448

449

450

451

452

453

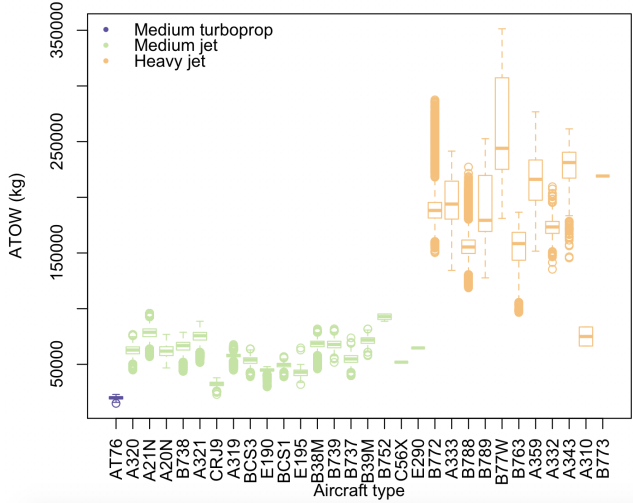


Figure 10. Boxplot of actual takeoff weight for each aircraft type.

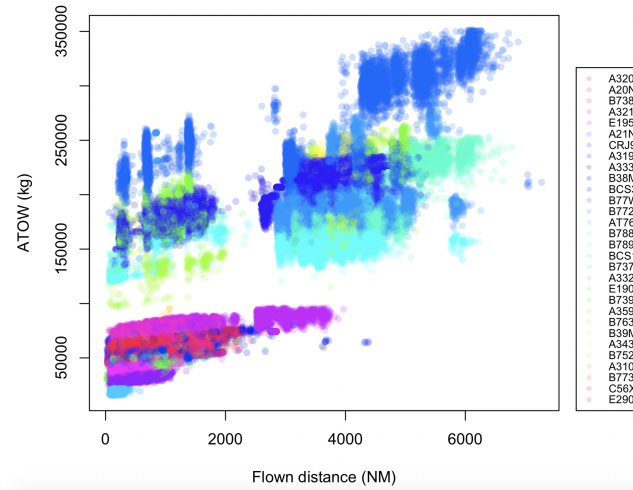


Figure 11. Scatterplot of the actual takeoff weight and distance flown for each aircraft type.

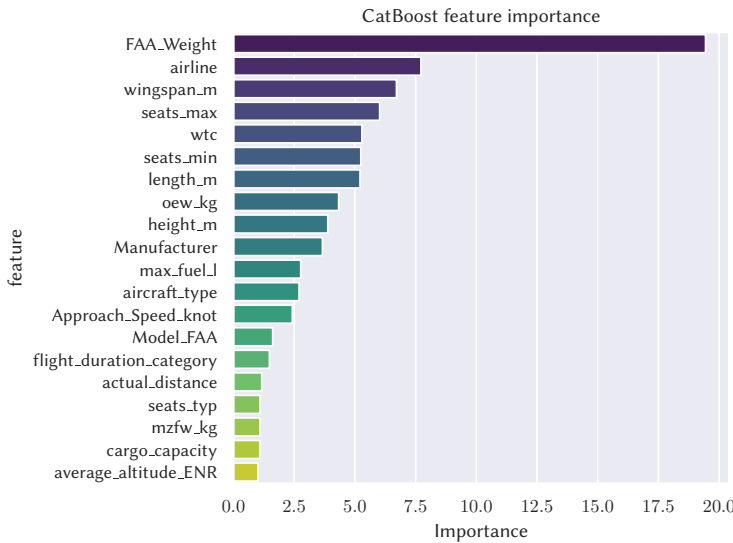
### 3.3 Feature Importance Analysis

Figure 12 presents the top 20 feature importances obtained from the trained CatBoost model, which achieved the best individual performance among the models tested. These importances were computed using the `PredictionValuesChange` method [21], indicating the average change in prediction if a feature's value is altered. As expected, aircraft features are among the most critical predictors overall. We also notice a significant contribution of the airline feature, emphasizing the impact of different operational policies and preferences on fuel loading. Regarding the trajectory features, the actual distance flown and the average en route altitude were the most important predictors, highlighting the influence of the horizontal and vertical profiles on fuel burn. A complete description of the features used can be found at the code repository.

454  
455  
456  
457  
458  
459  
460  
461  
462  
463

**Table 5.** Comparison of best hyperparameters, RMSE (estimated and actual), and Estimated MAPE for XGBoost, CatBoost, LightGBM, ANN, and the Ensemble models. The best RMSE and MAPE values are highlighted in bold and blue.

Algorithm	Best Hyperparameters	Estimated Test RMSE	Actual RMSE	Estimated Test MAPE
ANN	hidden_layers_size=[400, 300, 200], learning_rate=0.003	3,864.1	3,864.2	4.54%
SAINT	hidden_layers_size=[900, 400, 300], learning_rate=0.002	3,921.3	3,921.5	4.63%
CatBoost	learning_rate=0.01, reg_lambda=69.07, random_strength=16.35, depth=11, min_data_in_leaf=2, leaf_estimation_iterations=7	2,215.53	2,224.69	1.75%
LightGBM	learning_rate=0.01, reg_lambda=0.46, reg_alpha=0.17, min_child_weight=4, max_depth=13, colsample_bytree=0.60, subsample=1.0	2,506.43	2,519.17	2.50%
XGBoost	subsample=1.0, reg_lambda=0.46, reg_alpha=0.17, min_child_weight=4, max_depth=13, gamma=0.44, colsample_bytree=0.6	2,413.05	2,403.07	2.42%
Ensemble	weighted average=[8.65e-01, 1.34e-01, 4.77e-22, 1.24e-23, 1.63e-23]	<b>2,210.37</b>	<b>2,217.75</b>	<b>1.73%</b>

**Figure 12.** Top 20 feature importances for CatBoost.

### 3.4 Ablation Study

We present a comprehensive ablation study to quantify the impact of various feature groups and model components on the predictive performance of our ATOW estimation model. The study em-

467  
468

ploys a systematic approach to feature and component removal and evaluates the consequent changes in RMSE.

469  
470  
471  
472  
473

The ablation process started with our optimal ensemble model as the baseline and our best model when changing features. Features were categorized into five distinct groups: temporal, geographical, aircraft characteristics, operational, and meteorological. Each group was sequentially removed from the feature set, and the model was retrained and evaluated. Additionally, we assessed the impact of eliminating individual algorithms from the ensemble.

474  
475

Table 6 presents the results of the ablation study, showcasing the RMSE values and percentage changes relative to the baseline model for each ablated configuration.

**Table 6.** Ablation Study Results

Ablated Component	RMSE	Change in RMSE (%)
Baseline (Full Model)	2,217.75	0.00%
Temporal Features	2,354.97	+6.19%
Geographical Features	2,390.26	+7.77%
Aircraft Characteristics	2,266.96	+2.22%
Operational Features	2,759.18	+24.41%
Meteorological Features	2,249.29	+1.42%
XGBoost Algorithm	2,221.49	+0.16%
CatBoost Algorithm	2,969.49	+33.90%
LightGBM Algorithm	2,217.75	+0.00%
Neural Network	2,217.75	+0.00%
SAINT	2,217.75	+0.00%

476  
477  
478  
479  
480  
481  
482

The ablation study shows that the operational features processed from the ADB-S data exert the most substantial influence on model performance, with their removal resulting in a 24.41% increase in RMSE (from 2,217.75 to 2,759.18). This significant degradation in performance shows the crucial role of operational parameters in accurate ATOW prediction. Among the algorithmic components, the CatBoost algorithm demonstrates the highest individual impact when removed from the ensemble, as its removal leads to a substantial 33.90% increase in RMSE, given that it has the highest weight and the most contribution to the ensemble's predictive capability.

483  
484  
485  
486  
487

Geographical and temporal features also show notable importance, with their removal causing RMSE increases of 7.77% and 6.19%, respectively. This indicates that spatial and temporal context provides valuable information for ATOW prediction, though not as critical as operational characteristics. Aircraft characteristics contribute moderately to the model's performance, with their exclusion resulting in a 2.22% increase in RMSE.

488  
489  
490

Interestingly, meteorological features show relatively minimal impact, with only a 1.42% increase in RMSE when removed. This suggests that while weather conditions do influence ATOW predictions, their effect is less pronounced compared to other feature groups in our model.

488  
489  
490

In the context of model components, the results reveal varying degrees of importance among the different algorithms. While the removal of CatBoost significantly impacts performance, the XGBoost algorithm shows minimal effect (0.16% RMSE increase). The unchanged RMSE values (0.00% change) for LightGBM, Neural Network, and SAINT algorithms suggest these components might benefit from further optimization or may be redundant in the current ensemble configuration, and thus pruned.

491  
492  
493  
494  
495

These findings show the importance of careful feature engineering in ATOW prediction, particularly regarding operational parameters and geographical-temporal contexts. They also validate the

496  
497

efficacy of our ensemble approach, while highlighting potential areas for optimization, especially in the selection and integration of other different algorithmic components.

## 4. Conclusion

This study aimed to predict the aircraft's actual takeoff weight by employing machine learning techniques on large-scale open aviation data. We demonstrated that accurate predictive models can be developed for this essential operational parameter through extensive experimentation with various algorithms and feature engineering strategies. The results indicated that ensemble models combining CatBoost, LightGBM, XGBoost, and artificial neural networks achieved the best overall performance, with a root mean squared error of 2,217.75. Among individual models, the CatBoost algorithm was the strongest performer, achieving an RMSE of 2,224.69. The analysis shows the effectiveness of gradient-boosting methods in this domain.

The investigation into the importance of features revealed that aircraft type, airline and flight profile characteristics are essential in predicting takeoff weight. Incorporating detailed aircraft data significantly enhanced model performance, emphasizing the value of leveraging supplementary information beyond conventional aircraft type and category features. The ablation study confirmed that feature engineering was critical in improving accuracy, with distinct feature groups contributing uniquely to model effectiveness. These findings suggest that a rich feature set, including precise aircraft characteristics, is essential for building reliable models in aviation data contexts.

The current approach, while promising, has several limitations. The reliance on purely data-driven models does not fully account for the aerodynamic and operational complexities inherent in aircraft weight estimation. Additionally, gaps in data coverage, mainly due to limitations in ADS-B signals, may affect model generalization across diverse geographical regions. Future research could address these challenges by incorporating analytical models that draw on aerodynamic principles and operational knowledge, integrating physics-based insights with machine learning. Such integration could provide physical constraints that enhance the reliability of the models. Additionally, exploring supplementary datasets, such as detailed aircraft specifications, meteorological data, and operational parameters, could further enrich feature sets, leading to more accurate predictions. Exploring advanced machine learning architectures and optimization methods could also contribute to refined predictions. Evaluating model performance across diverse operational conditions and extending the methodology to include other flight phases would enhance the applicability of these models in real-world air traffic management.

This work contributes to the broader aviation research community by demonstrating that machine learning methods can estimate aircraft takeoff weight using openly available data, achieving good performance. The developed models and methodologies lay a foundation for further advancements in aircraft weight estimation, with potential applications covering trajectory prediction and optimization and aviation's environmental impact assessment.

## Acknowledgement

Marcos Maximo thanks the support from CNPq – National Research Council of Brazil through the grant 307525/2022-8. Carolina Rutili thanks the support from Embraer through a scholarship associated with the Flight and Mobility Innovation Center (FLYMOV).

## Author contributions

- Mayara C. R. Murça: Conceptualization, Formal Analysis, Investigation, Methodology, Supervision, Project Administration, Visualization, Writing (Original Draft), Writing (Review and Edit-

- ing). 541
- Marcos R. O. A. Maximo: Conceptualization, Data Curation, Methodology, Software, Supervision, Project Administration, Visualization, Writing (Original Draft), Writing (Review and Editing). 542
  - Joao P. A. Dantas: Data Curation, Formal Analysis, Investigation, Methodology, Software, Validation, Visualization, Writing (Original Draft), Writing (Review and Editing). 543
  - João B. T. Szenczuk: Data Curation, Formal Analysis, Investigation, Methodology, Visualization, Writing (Original Draft). 544
  - 545
  - Carolina R. Lima: Methodology, Software, Investigation, Writing the draft and reviewing. 546
  - Lucas O. Carvalho: Data Curation, Formal Analysis, Investigation, Methodology, Writing (Original Draft). 549
  - 550
  - Gabriel A. Melo: Data Curation, Methodology, Software, Writing (Original Draft). 551

## Reproducibility statement

The open-source code for this research is available at <https://github.com/marcosmaximo/prc-challenge-ita>. 552

## References

- [1] International Civil Aviation Organization. *Global Air Navigation Plan (Doc 9750, 6<sup>th</sup> Edition)*. ICAO, 2019. 556
- [2] M. Murça and M. Oliveira. “A data-driven probabilistic trajectory model for predicting and simulating terminal airspace operations”. In: *2020 AIAA/IEEE 39th Digital Avionics Systems Conference (DASC)*. 2020, pp. 1–7. doi: 10.1109/DASC50938.2020.9256644. 557
- [3] S. Mondoloni and N. Rozen. “Aircraft trajectory prediction and synchronization for air traffic management applications”. In: *Progress in Aerospace Sciences* 119 (2020), p. 100640. doi: <https://doi.org/10.1016/j.paerosci.2020.100640>. 558
- [4] Y. Chati and H. Balakrishnan. “Statistical modeling of aircraft engine fuel flow rate”. In: *30th Congress of the International Council of the Aeronautical Science*. 2016. 559
- [5] C. Huang and X. Cheng. “Estimation of aircraft fuel consumption by modeling flight data from avionics systems”. In: *Journal of Air Transport Management* 99 (2022), p. 102181. doi: <https://doi.org/10.1016/j.jairtraman.2022.102181>. 560
- [6] S. Badrinath, J. Abel, H. Balakrishnan, E. Joback, and T. Reynolds. “Spatial modeling of airport surface fuel burn for environmental impact analyses”. In: *Journal of Air Transportation* 31.3 (2023), pp. 85–97. doi: 10.2514/1.D0294. 561
- [7] J. Sun, L. Basora, X. Olive, M. Strohmeier, M. Schäfer, I. Martinovic, and V. Lenders. “Open-Sky Report 2022: Evaluating aviation emissions using crowdsourced open flight data”. In: *2022 IEEE/AIAA 41st Digital Avionics Systems Conference (DASC)*. 2022, pp. 1–8. doi: 10.1109/DASC55683.2022.9925852. 562
- [8] R. Teoh, Z. Engberg, M. Shapiro, L. Dray, and M. Stettler. “The high-resolution Global Aviation emissions Inventory based on ADS-B (GAIA) for 2019–2021”. In: *Atmospheric Chemistry and Physics* 24.1 (2024), pp. 725–744. doi: 10.5194/acp-24-725-2024. 563
- [9] R. Coppenbarger. “En route climb trajectory prediction enhancement using airline flight-planning information”. In: *Guidance, Navigation, and Control Conference and Exhibit*. 2019. doi: 10.2514/6.1999-4147. 564
- [10] R. Alligier, D. Gianazza, and N. Durand. “Learning the aircraft mass and thrust to improve the ground-based trajectory prediction of climbing flights”. In: *Transportation Research Part C: Emerging Technologies* 36 (2013), pp. 45–60. doi: <https://doi.org/10.1016/j.trc.2013.08.006>. 565

- [11] OpenSky Network. *Open Air Traffic Data for Research*. [Online; accessed September 2024]. URL: <https://opensky-network.org/>. 585  
586
- [12] R. Alligier. “Predictive Distribution of Mass and Speed Profile to Improve Aircraft Climb Prediction”. In: *Journal of Air Transportation* 28.3 (2020), pp. 114–123. doi: 10.2514/1.D0181. 587  
588
- [13] J. Sun, J. Ellerbroek, and J. Hoekstra. “Modeling and Inferring Aircraft Takeoff Mass from Runway ADS-B Data”. In: *7th International Conference on Research in Air Transportation*. 2016. 589  
590
- [14] J. Sun, J. Ellerbroek, and J. Hoekstra. “Aircraft initial mass estimation using Bayesian inference method”. In: *Transportation Research Part C: Emerging Technologies* 90 (2018), pp. 59–73. doi: 591  
592  
593  
<https://doi.org/10.1016/j.trc.2018.02.022>. 594  
595
- [15] Eurocontrol. *Performance Review Commission (PRC) Data Challenge*. [Online; accessed September 2024]. URL: <https://ansperformance.eu/study/data-challenge/>. 596  
597
- [16] Eurocontrol. *Vertical flight efficiency @ airports*. [Online; accessed October 2024]. URL: <https://ansperformance.eu/efficiency/vfe/>. 598  
599
- [17] S. Salgueiro, J. L. Huynh, and R. J. Hansman. “Aircraft takeoff and landing weight estimation from surveillance data”. In: *AIAA SCITECH 2022 Forum*. 2022. doi: 10.2514/6.2022-1307. 600  
601
- [18] L. Grinsztajn, E. Oyallon, and G. Varoquaux. “Why do tree-based models still outperform deep learning on typical tabular data?” In: *Advances in Neural Information Processing Systems*. Ed. by S. Koyejo, S. Mohamed, A. Agarwal, D. Belgrave, K. Cho, and A. Oh. Vol. 35. Curran Associates, Inc., 2022, pp. 507–520. URL: [https://proceedings.neurips.cc/paper\\_files/paper/2022/file/0378c7692da36807bdec87ab043cdadc-Paper-Datasets\\_and\\_Benchmarks.pdf](https://proceedings.neurips.cc/paper_files/paper/2022/file/0378c7692da36807bdec87ab043cdadc-Paper-Datasets_and_Benchmarks.pdf). 602  
603  
604
- [19] L. Grinsztajn, E. Oyallon, and G. Varoquaux. “Why do tree-based models still outperform deep learning on typical tabular data?” In: *Proceedings of the 36th International Conference on Neural Information Processing Systems*. NIPS ’22. New Orleans, LA, USA: Curran Associates Inc., 2024. ISBN: 9781713871088. 605  
606  
607
- [20] T. Chen and C. Guestrin. “XGBoost: A Scalable Tree Boosting System”. In: *Proceedings of the 22nd ACM SIGKDD International Conference on Knowledge Discovery and Data Mining*. KDD ’16. San Francisco, California, USA: Association for Computing Machinery, 2016, pp. 785–794. ISBN: 9781450342322. doi: 10.1145/2939672.2939785. URL: <https://doi.org/10.1145/2939672.2939785>. 608  
609  
610  
611  
612  
613
- [21] J. T. Hancock and T. M. Khoshgoftaar. “CatBoost for big data: an interdisciplinary review”. In: *Journal of big data* 7.1 (2020), p. 94. 614  
615
- [22] G. Ke, Q. Meng, T. Finley, T. Wang, W. Chen, W. Ma, Q. Ye, and T-Y Liu. “LightGBM: A Highly Efficient Gradient Boosting Decision Tree”. In: *Advances in neural information processing systems*. 2017, pp. 3146–3154. 616  
617  
618
- [23] A. A. Ibrahim, R. L. Ridwan, M. M. Muhammed, R. O. Abdulaziz, and G. A. Saheed. “Comparison of the CatBoost classifier with other machine learning methods”. In: *International Journal of Advanced Computer Science and Applications* 11.11 (2020). 619  
620  
621
- [24] T. Akiba, S. Sano, T. Yanase, T. Ohta, and M. Koyama. “Optuna: A Next-generation Hyperparameter Optimization Framework”. In: *Proceedings of the 25th ACM SIGKDD International Conference on Knowledge Discovery & Data Mining*. KDD ’19. Anchorage, AK, USA: Association for Computing Machinery, 2019, pp. 2623–2631. ISBN: 9781450362016. doi: 10.1145/3292500.3330701. URL: <https://doi.org/10.1145/3292500.3330701>. 622  
623  
624  
625  
626  
627
- [25] T. G. Dietterich. “Ensemble methods in machine learning”. In: *International workshop on multiple classifier systems*. Springer. 2000, pp. 1–15. 628